

Internal structure of clusters in $^{112-122}\text{Ba}$ nuclei within relativistic mean field theory

M. Bhuyan^{1,2}, S.K. Patra¹, P. Arumugam³, and Raj K. Gupta⁴

¹*Institute of Physics, Sachivalaya Marg, Bhubaneswar-751 005, India,*

²*School of Physics, Sambalpur University, Jyotivihar, Burla-768 019, India,*

³*Department of Physics, Indian Institute of Technology, Roorkee-247 667, India,*

⁴*Department of Physics, Panjab University, Chandigarh-160 014, India.*

(Dated: June 26, 2018)

We study the clustering structure and the internal or sub-structure of clusters in $^{112-122}\text{Ba}$ nuclei within the framework of relativistic mean field theory in an axially deformed cylindrical co-ordinate. We calculate the total density distribution, and the individual neutrons and protons density distributions. From the analysis of the clustering configurations of the density distributions of various shapes, we find different sub-structures inside the Ba nuclei considered here. The important step, carried out for the first time, is the counting of number of protons and neutrons present in the clustering region(s). ^{12}C is shown to constitute the cluster configuration of Ba nuclei in most cases, with $^2,^3\text{H}$ and ^4He constituting the neck between two fissioning symmetrical fragments.

PACS numbers: 21.10.Dr, 21.60.-n, 21.60.Jz, 21.60.Gx, 24.10.Jv, 23.70.+j

I. INTRODUCTION

Instabilities of "stable" nuclei against exotic cluster decays were first studied by one of us (RKG) and collaborators [1, 2, 3, 4] for the neutron-deficient $^{108-116}\text{Xe}$, $^{112-120}\text{Ba}$, $^{116-124}\text{Ce}$, $^{120-124}\text{Nd}$, $^{124-128}\text{Sm}$, and $^{128-132}\text{Gd}$ and neutron-rich ^{146}Ba , ^{152}Ce , ^{156}Nd , ^{160}Sm , and ^{164}Gd nuclei, on the basis of the preformed cluster model (PCM) of Malik and Gupta [5, 6] (see, also the works of other authors [7, 8]). The $N = Z$, α -nuclei ^8Be , ^{12}C , ^{16}O , ^{20}Ne , ^{24}Mg , and ^{28}Si are predicted to be the most probable emitters from neutron-deficient parents, with a much smaller decay half-life compared to $N > Z$ clusters predicted preferably or observed from neutron-rich parents (e.g., ^{14}C from ^{146}Ba or ^{222}Ra with ^{132}Sn or ^{208}Pb as daughter, respectively). Thus, other than α particle, ^{12}C decay of $^{112-120}\text{Ba}$ nuclei is shown to be the most probable one with ^{100}Sn and its heavier isotopes as the daughter nuclei. The ground-state decay of Ba, however, could not be established as yet [9, 10], and a new phenomenon of intermediate mass fragments (IMFs) with $3 \leq Z \leq 9$, also referred to as 'clusters' or 'complex fragments', is observed to be emitted from the compound nucleus $^{116}\text{Ba}^*$ formed in $^{58}\text{Ni} + ^{58}\text{Ni} \rightarrow ^{116}\text{Ba}^*$ reactions at both the high [11, 12] and medium energies [13, 14]. The measured IMF cross-section σ_{IMF} for the $^{116}\text{Ba}^*$ decay at all the above mentioned medium and high energies are so far understood only on the preformed-clusters (PCM) based dynamical cluster-decay model (DCM) of one of us (RKG) and collaborators [15]. The DCM describes the $^{116}\text{Ba}^*$ data on σ_{IMF} reasonably well, and predicts an additional fusion-fission of $^{116}\text{Ba}^*$ which consists of fragments at the heavy end of symmetric and near symmetric division ($14 \leq Z \leq 28$), very recently observed at GANIL [16] for the decays of $^{118,122}\text{Ba}^*$ nuclei produced in $^{78,82}\text{Kr} + ^{40}\text{Ca}$ reactions at a lower incident energy, and also explained more recently [17] on DCM. It should thus be interesting to see if mean-field approaches, such as the relativistic mean field model, support such a clustering structure for the ground and/ or excited states of Ba nuclei.

Relativistic mean field (RMF) calculations for light nuclei [18] have very successfully shown the $\alpha - \alpha$ clustering in ^8Be ,

a benchmark nucleus, and the α -clustering and halo structures of $(\alpha + \alpha)$ -core or $(\alpha + \alpha + p)$ -core plus xn for the stable and exotic Be and B nuclei. For the $N=Z$, α -nuclei ^{12}C and ^{16}O , the RMF formalism gives the several known ground-state (g.s.) structures such as the 3α -equilateral triangle (co-existing with spherical shape) and 4α -tetrahedron or kite-like, plus the 3α - and 4α -linear chains for their excited states. Also, both α - and non- α -cluster structures, like $^{10}\text{B} + ^{10}\text{B}$, $^{12}\text{C} + ^{12}\text{C}$, $^{12}\text{C} + \alpha + ^{12}\text{C}$ and $^{16}\text{O} + ^{16}\text{O}$, and 5α -trigonal bipyramid and pentagonal bipyramid (hollow sphere) are obtained for ^{20}Ne to ^{32}S nuclei, but *no* 5α , 6α chains, etc., are seen. Furthermore, ^{56}Ni shows [19] a preferred $N=Z$, α -nucleus clustering for states with deformations up to hyper-deformation ($\beta \leq 2.45$). Similarly, for heavy actinides (^{222}Ra , ^{232}U , ^{236}Pu and ^{242}Cm), the RMF gives [20] not only the $N \approx Z$, α -like clustering in the g.s. but also the exotic $N \neq Z$ clustering in excited states. Signatures of clustering structure in RMF calculations of super-heavy $Z=114$ and 120 , $N=172-184$ nuclei [20, 21] are also obtained in terms of exotic $N \neq Z$ clusters at the centre of their super-deformed g.s. or the clustering in to two large and some small pieces is universal for all super-deformed ground states in $Z=120$ nuclei. The super-superheavy $^{238}\text{U} + ^{238}\text{U} \rightarrow ^{476}184^*$ nucleus also supports the clustering phenomenon, with a kind of triple fission of an exotic cluster in the neck region of two equal fragments of $N=Z$ matter [22]. The actual internal or sub-structure structure of the clusters, however, was not determined in these calculations, which is one of the aims of the present study.

Taking RMF model as an established tool for the cluster structure in nuclei, in this paper we demonstrate its application to medium-heavy $^{112-122}\text{Ba}$ nuclei, with an additional attempt to determine for the first time the internal structure(s) of cluster(s), i.e., the number of protons and neutrons in a cluster. The paper is so designed that Section II describes the relativistic mean field theory, and Section III gives the results obtained from our calculation. Finally a brief summary and concluding remarks are given in Section IV.

II. THE RELATIVISTIC MEAN FIELD (RMF) METHOD

The relativistic Lagrangian density for a nucleon-meson many-body system [23, 24]

$$\begin{aligned}
\mathcal{L} = & \bar{\psi}_i \{ i\gamma^\mu \partial_\mu - M \} \psi_i + \frac{1}{2} \partial^\mu \sigma \partial_\mu \sigma - \frac{1}{2} m_\sigma^2 \sigma^2 \\
& - \frac{1}{3} g_2 \sigma^3 - \frac{1}{4} g_3 \sigma^4 - g_s \bar{\psi}_i \psi_i \sigma - \frac{1}{4} \Omega^{\mu\nu} \Omega_{\mu\nu} \\
& + \frac{1}{2} m_w^2 V^\mu V_\mu + \frac{1}{4} c_3 (V_\mu V^\mu)^2 - g_w \bar{\psi}_i \gamma^\mu \psi_i V_\mu \\
& - \frac{1}{4} \vec{B}^{\mu\nu} \cdot \vec{B}_{\mu\nu} + \frac{1}{2} m_\rho^2 \vec{R}^\mu \cdot \vec{R}_\mu - g_\rho \bar{\psi}_i \gamma^\mu \vec{\tau} \psi_i \cdot \vec{R}_\mu \\
& - \frac{1}{4} F^{\mu\nu} F_{\mu\nu} - e \bar{\psi}_i \gamma^\mu \frac{(1 - \tau_{3i})}{2} \psi_i A_\mu. \quad (1)
\end{aligned}$$

From this Lagrangian we obtain the field equations for the nucleons and mesons. These equations are solved by expanding the upper and lower components of the Dirac spinors and the boson fields in an axially deformed harmonic oscillator basis with an initial deformation β_0 . The set of coupled equations is solved numerically by a self-consistent iteration method. The centre-of-mass motion (c.m.) energy correction is estimated by the usual harmonic oscillator formula $E_{c.m.} = \frac{3}{4} (41A^{-1/3})$. The quadrupole deformation parameter β_2 is evaluated from the resulting proton and neutron quadrupole moments, as $Q = Q_n + Q_p = \sqrt{\frac{16\pi}{5}} (\frac{3}{4\pi} AR^2 \beta_2)$. The root mean square (rms) matter radius is defined as $\langle r_m^2 \rangle = \frac{1}{A} \int \rho(r_\perp, z) r^2 d\tau$; here A is the mass number, and $\rho(r_\perp, z)$ is the deformed density. The total binding energy and other observables are also obtained by using the standard relations, given in [24]. We use the well known NL3 parameter set [25]. This set reproduces the properties of stable nuclei. As outputs, we obtain different potentials, densities, single-particle energy levels, radii, quadrupole deformations and the binding energies. For a given nucleus, the maximum binding energy corresponds to the ground state and other solutions are obtained as various excited intrinsic states.

The density distribution of nucleons play the prominent role for studying the internal structure of a nucleus. For a different quadrupole deformation, the density distribution $\rho(r_\perp, z)$ inside the nucleus must vary. For example, the $\rho(r_\perp, z)$ for a spherical nucleus is symmetrical in (ρ, z) -plane. However, it is highly asymmetric for a largely deformed nucleus. Knowing the density distribution of the spherical or (oblate/prolate) deformed configuration, we can calculate the number of nucleons for each configuration, defined as

$$n = \int_{z_1}^{z_2} \int_{r_1}^{r_2} \rho(r_\perp, z) d\tau, \quad (2)$$

with n as number of neutrons N , protons Z or mass A . Though a straight forward calculation, this is being carried out here for the first time.

III. CALCULATIONS AND RESULTS

A. Ground state properties of Ba nuclei using the RMF formalism

1. Potential Energy Surface

We first calculate the potential energy surface (PES) by using the RMF formalism in a constrained calculation [26, 27, 28, 29, 30], i.e., instead of minimizing the H_0 , we have minimized $H' = H_0 - \lambda Q_2$, with λ as a Lagrange multiplier and Q_2 , the quadrupole moment. The term H_0 is the Dirac mean field Hamiltonian for RMF model (the notations are standard and its form can be seen in Refs. [24, 28, 30]). In other words, we get the constrained binding energy from $BE_c = \sum_{ij} \frac{\langle \psi_i | H_0 - \lambda Q_2 | \psi_j \rangle}{\langle \psi_i | \psi_j \rangle}$ and the free energy from $BE = \sum_{ij} \frac{\langle \psi_i | H_0 | \psi_j \rangle}{\langle \psi_i | \psi_j \rangle}$. The converged free energy solution does not depend on the initial guess value of the basis deformation β_0 as long as it is nearer to the minimum in PES. However, it converges to some other local minimum when β_0 is drastically different, and in this way we evaluate a different intrinsic isomeric state for a given nucleus.

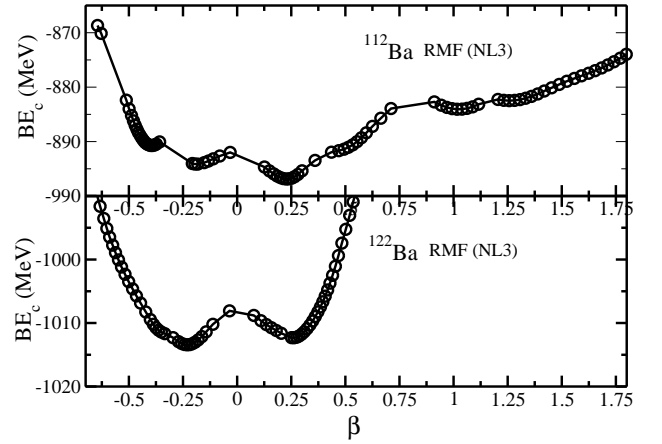


FIG. 1: The potential energy surfaces for ^{112}Ba and ^{122}Ba nuclei, i.e. constrained binding energy (BE_c) as a function of quadrupole deformation parameter in RMF(NL3) calculations.

The PES for the representative ^{112}Ba and ^{122}Ba nuclei are shown in Fig. 1 for a wide range of β_2 starting from oblate to prolate deformation. The upper panel is for ^{112}Ba and the lower one for ^{122}Ba . For ^{112}Ba , we notice the minima are around $\beta_2 = -0.39, -0.20, 0.23, 1.02$ and 1.20 , corresponding to binding energy $BE_c = 890.6, 894.2, 896.7, 884.2$ and 882.7 MeV, respectively, and their energy differences between the nearest consecutive minima are 3.60, 2.50, 12.93 and 1.52 MeV. However, in case of ^{122}Ba , only two minima exist around $\beta_2 = -0.23$ and 0.26 at $BE_c = 1013.4$ and 1012.4 MeV. The intrinsic energy difference between these two configurations is 1.03 MeV. From this figure, it is clear that there exists two identical major minima at $\beta_2 \approx -0.23$ and 0.23 in

TABLE I: The RMF(NL3) results of binding energy, the quadrupole deformation parameter β_2 , and the root mean square radii of charge r_c and matter r_m for the $^{112-122}\text{Ba}$ nuclei. The energy is in MeV, and radii in fm. The experimental data are from [31, 32], and the binding energies marked with star (*) are the extrapolated values. The finite range droplet model (FRDM) binding energy and β_2 are taken from [33] and the theoretical charge radius r_c is from Hartree-Fock-BCS (HFBCS) method [34]. No experimental data are available for r_c .

Nucleus	BE		r_{rms} : RMF(NL3)		β_2		BE	r_c	β_2
	RMF(NL3)	Expt.	r_m	r_c	RMF(NL3)	Expt.	FRDM	HFBCS	FRDM
^{112}Ba	860.79		4.80	4.99	-0.39				
	893.50		4.65	4.79	-0.17				
	895.38		4.62	4.74	0.24		894.89	4.72	0.21
	882.36		5.35	5.48	1.24				
	897.33		12.17	12.21	10.71				
^{114}Ba	918.10		4.78	4.90	-0.39				
	920.13	922.26	4.65	4.75	0.24		921.27	4.74	0.24
	909.35		5.33	5.45	1.19				
^{116}Ba	920.61		12.16	12.20	10.58				
	943.66	947.024*	4.80	4.90	-0.39				
	945.70		4.71	4.79	0.36		946.85	4.78	0.28
	934.15		5.36	5.46	1.20				
^{118}Ba	942.38		12.13	12.16	10.40				
	969.16		4.73	4.81	-0.24				
	971.38	971.022*	4.75	4.82	0.33		970.75	4.80	0.29
^{120}Ba	962.45		12.11	12.13	10.24				
	991.64		4.75	4.81	-0.23				
	993.94	993.600	4.77	4.83	0.32		993.44	4.82	0.28
^{122}Ba	975.04		12.55	12.58	10.97				
	1013.53		4.77	4.82	-0.22				
	1015.52	1015.499	4.80	4.84	0.32	0.354	1015.21	4.81	0.27
	999.40		12.09	12.10	9.95				

both the ^{112}Ba and ^{122}Ba nuclei. A further investigation of the diagram shows that actually the multi-minima structure of ^{112}Ba disappears gradually with the increase of mass number in the isotopic chain of Ba, and reaches to only two minima configuration, one oblate and another prolate, at mass number $A=122$.

2. Binding Energies and Quadrupole Deformation Parameter

The binding energies and quadrupole deformation parameters β_2 for $^{112-122}\text{Ba}$ isotopes are evaluated for the ground as well as intrinsic excited states. The obtained results are tabulated in Table I, together with the experimental or extrapolated values, wherever available. The experimental value of g.s. β_2 is available for ^{122}Ba only. Since the neutron-deficient $^{112-120}\text{Ba}$ isotopes lie near the proton drip-line, their deformation parameters are not yet known. Table I shows that both the g.s. binding energies, charge radius (r_c) and β_2 values agree well with the experimental data and with the theoretical calculations [33, 34].

As discussed above, lighter Ba isotopes have several intrinsic minima, where each minimum corresponds to a deformation and a binding energy. The largest binding energy minimum corresponds to the ground state and all other minima are the excited intrinsic states. In this way, the ground state β_2 is 0.24 for ^{112}Ba . Similarly, the g.s. deformations for ^{114}Ba , ^{116}Ba , ^{118}Ba , ^{120}Ba and ^{122}Ba are 0.24, 0.36, 0.33, 0.32 and 0.32, respectively. All other intrinsic state deforma-

tions are also listed in Table I. For $^{112,114,116}\text{Ba}$ nuclei we get a solution at a highly deformed configuration of $\beta_2 \sim 1.2$, whereas this hyper-deformed minimum is washed out with increase of mass number in the Ba isotopic chain. This means there is no hyper-deformed solutions for $^{118-122}\text{Ba}$ (see also, Fig. 4 where such highly deformed configurations are shown only for $^{112,114,116}\text{Ba}$). If the nucleus is further deformed ($\beta_2 \sim 10$), it breaks into two fragments (see also Fig. 5) with a separation radius r_m of about 12 fm. An analysis of this structure shows two distinct (fission-like) fragments connected with a thin density distribution of nucleons, which can be considered like a very thin neck. We find that the composition of the (connecting) neck region is an isotopic chain of hydrogen or helium nuclei $^2,^3\text{H}$ and ^4He (discussed below).

3. The root-mean-square radii r_{rms}

In this subsection, we discuss our calculation on root mean square (rms) radii of matter distribution, with various quadrupole deformations from oblate to prolate and then from super-deformation to hyper-deformation. The matter rms radius r_m and charge distribution rms radius r_c are listed in Table I for different β_2 values. From Table I, it is observed that the r_m increases with increase of quadrupole deformation. Finally, both r_m and r_c show a large extension of about 12 fm at $\beta_2 \sim 10.5$. As already pointed out above, at this point of deformation, the two fragments get separated from each other leaving a thin density distribution of matter in between the two

fragments or clusters.

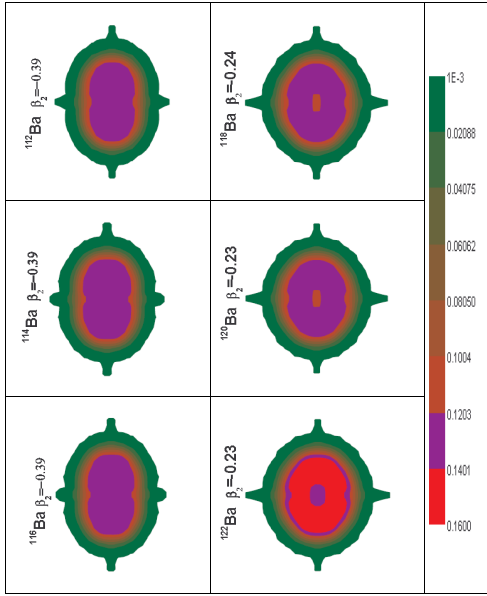


FIG. 2: (Color on line) The cluster configurations of $^{112-122}\text{Ba}$ for the oblate states in RMF(NL3).

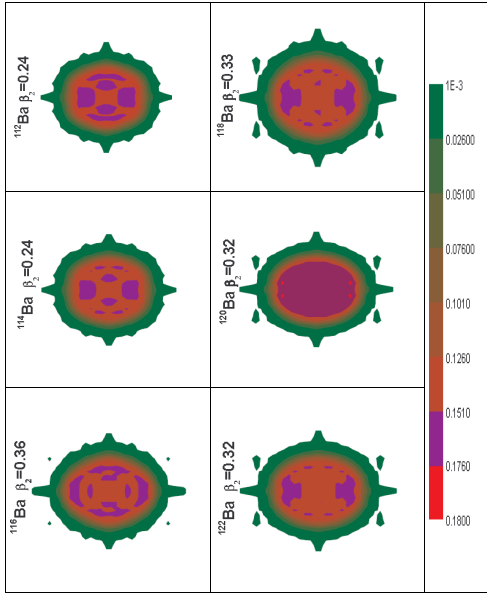


FIG. 3: (Color on line) The cluster configurations of $^{112-122}\text{Ba}$ for the ground states in RMF(NL3).

B. Cluster configurations in $^{112-122}\text{Ba}$ nuclei

Figures 2 to 5 show the density plots for all the possible solutions, starting from oblate to prolate deformations of the

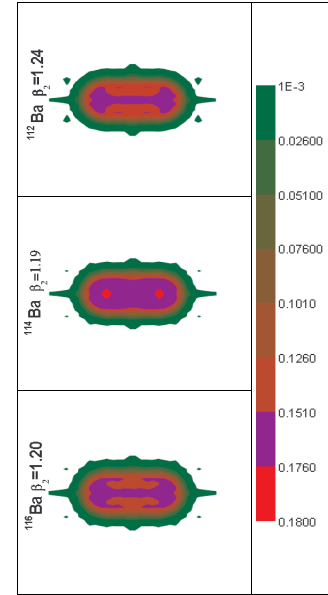


FIG. 4: (Color on line) The cluster configurations of $^{112-122}\text{Ba}$ for the prolate states in RMF(NL3).

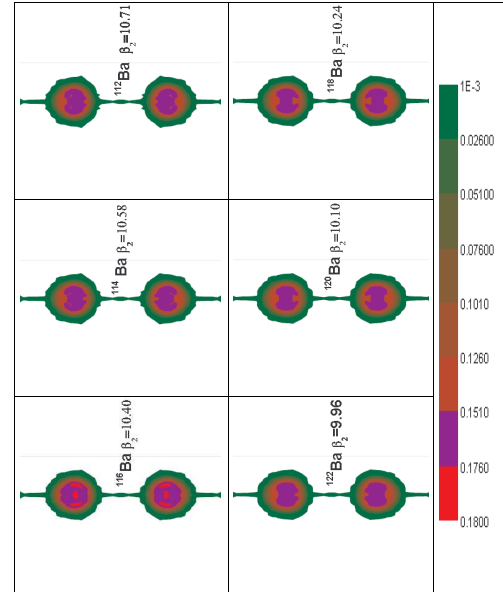


FIG. 5: (Color on line) The cluster configurations of $^{112-122}\text{Ba}$ for the hyper-deformed states in RMF(NL3).

Ba isotopic chain. Fig. 2 gives the density distributions for $^{112-122}\text{Ba}$ for the oblate state solutions around the deformation parameter $\beta_2 \sim -0.35$, and Figs. 3, 4 and 5 show, respectively, the prolate state solutions of $^{112-122}\text{Ba}$ around $\beta_2 \sim 0.25, 1.1$ and 10.5 . From these graphs the clustering structures in these nuclei are quite evident. Considering the colour code, starting from deep black with maximum to white (or light gray) bearing the minimum density, one can analyse

the distribution of nucleons inside the various isotopes at various shapes. In Fig. 2 the minimum density for the oblate-state starts from 0.001 fm^{-3} and goes up to maximum 0.16 fm^{-3} , but in case of the prolate-states in Figs. 3, 4 and 5, it starts from 0.001 fm^{-3} and goes up to 0.18 fm^{-3} , which shows that the size of cluster nucleus is smaller in the oblate-state than that of the prolate-state. A careful inspection of the density distributions in different regions of the nucleus clearly shows the formation of various cluster(s) inside the nuclei, which are listed in Table II as clusters I, II or III for a given deformation β_2 .

Further, if we increase the value of deformation parameter β_2 to ~ 10.4 - 10.7 or more, the nucleus gets separated into two fragments with a neck formation as shown in Fig. 5 for the isotopic chain of $^{112-122}\text{Ba}$ nuclei. Another prominent observation is that there is no configuration of deformation parameter $\beta_2 \sim 1.2$ in case of $^{118-122}\text{Ba}$, similar to what is shown in Fig. 4 for lighter mass Ba isotopes. If we compare the cluster configurations of each nucleus, it is clear that there is a gradual change in the configuration inside the nucleus, i.e., the clusters inside the nucleus for different β_2 values are distinct from each other, and for each isotope of $^{112-122}\text{Ba}$ chain.

TABLE II: The number of nucleons $A_{clus.}$, the protons $Z_{clus.}$, and neutrons $N_{clus.}$ in a cluster inside the $^{112-122}\text{Ba}$ nuclei for different solutions of deformations β_2 obtained from the RMF(NL3) formalism. The range of the cluster ($r_1, r_2; z_1, z_2$) are in fm.

Nucleus	β_2	Cluster No. range ($r_1, r_2; z_1, z_2$)	$A_{clus.}$	$Z_{clus.}$	$N_{clus.}$	Cluster
^{112}Ba	-0.39	I (-0.7,0.7;-3.0,-1.7)	11.6	5.6	6.0	^{12}C
	0.24	I (1.9,4.5;-1.5,1.5)	36.0	17.7	18.3	^{36}Ar
^{114}Ba		II (-1.3,1.3;-2.6,-1.2)	13.0	6.3	6.7	^{13}C
	10.71	I (-6.3,6.3;-3.5,3.5)	1.6	0.7	0.8	^2H
	0.24	I (2.1,4.6;-1.5,1.5)	34.7	16.9	17.9	^{35}Cl
		II (-1.1,1.1;1.2,2.5)	12.6	6.1	6.4	^{13}C
^{116}Ba		III (0.7,2.0;3.3,3.7)	2.3	1.1	1.2	^2H
	1.19	I (3.9,5.4;-0.7,0.7)	8.4	4.1	4.3	^8Be
	10.58	I (-6.6,6.3;-3.8,3.8)	2.2	1.1	1.1	^2H
	0.36	I (4.4,6.2;-1.6,1.6)	25.3	12.3	13.1	^{25}Mg
^{118}Ba		II (2.6,3.4;-0.9,0.9)	6.1	2.8	3.4	^6Li
	10.40	I (11.0,12.2;-0.8,0.8)	7.5	3.7	3.8	^8Be
		II (9.9,12.8;2.3,2.9)	6.6	3.2	3.4	^6Li
		III (-6.1,6.1;-3.4,3.4)	1.9	0.9	1.0	^2H
^{120}Ba	-0.24	I (-0.6,0.6;-1.2,1.2)	12.85	6.9	5.9	^{13}C
	0.33	I (2.5,5.5;-1.6,1.6)	42.0	19.9	22.2	^{42}Ca
		II (0.7,2.0;3.3,3.6)	1.7	0.8	0.9	^2H
		III (-0.4,0.4;-2.1,-1.6)	1.6	0.7	0.8	^2H
^{122}Ba	10.24	I (-6.2,6.2;-3.7,3.7)	2.8	1.2	1.6	^3H
	-0.23	I (-0.6,0.6;-1.2,1.2)	12.9	5.8	7.1	^{13}C
	0.32	I (-5.5,-5.0;-0.7,-1.2)	0.9	0.3	0.6	^1H
^{122}Ba	10.97	I (-6.3,6.3;-4.3,4.3)	3.8	1.6	2.1	^4He
	-0.22	I (-1.0,1.0;-1.5,1.5)	24.4	11.2	13.2	^{23}Na
	0.32	I (2.5,5.3;-1.7,1.7)	42.6	19.7	22.8	^{43}Ca
		II (-2.0,-0.8;3.4,3.7)	1.6	0.7	0.8	^2H
	9.96	I (-6.1,6.1;-3.7,3.7)	2.4	1.0	1.4	^2H

C. Counting of nucleons in clusters formed inside the $^{112-122}\text{Ba}$ nuclei

In this subsection, we count the number of nucleons in different clusters formed inside the $^{112-122}\text{Ba}$ isotopic chain, listed in the Table II. The density distributions of these clusters, obtained from the RMF(NL3) formalism for different solutions of deformation parameters β_2 from oblate to prolate configurations, are already shown above in Figs. 2 to 5. From these distribution plots of each oblate or prolate configuration, we find the number of nucleons by using the general formula in Eq. (2), for not only the total nucleons (using total density distribution of the nucleus) but also for protons and neutrons (using individual density distributions), which is listed in the Table II. For this calculation, we first find the range of the integral, i.e., the lower and the upper limits of the axes (r and z) from the plots in Figs. 2 to 5, and then evaluate the integral for each case.

Table II first shows that the number of protons and neutrons from the individual density distributions gives the total number of nucleons which is calculated here from the total density distribution of the nucleus for each isotope of Ba with different β_2 solutions. Secondly, the internal cluster configuration of $^{112-122}\text{Ba}$ nuclei contain ^{12}C or ^{13}C as the most common cluster. For the oblate-state ($\beta_2 \sim 0.35$, Fig. 2), the density distribution is uniform for $^{114,116}\text{Ba}$ isotopes, but in cases of $^{112,118,120}\text{Ba}$ isotopes we find a ^{12}C or ^{13}C cluster, and for ^{122}Ba a ^{23}Na cluster. The ground-state density distributions (around $\beta_2 \sim 0.25$, Fig. 3) of $^{112,114}\text{Ba}$ contain ^{13}C cluster, but $^{116-122}\text{Ba}$ contain clusters of some other elements like ^6Li and $^1,2\text{H}$. The density distributions for the prolate-state ($\beta_2 \sim 1.2$, Fig. 4) are again uniform for the isotopes $^{112,116}\text{Ba}$, but show ^8Be cluster configuration for ^{114}Ba . Note that there are no solutions for $\beta_2 \sim 1.2$ for the isotopic chain $^{118-122}\text{Ba}$. For the very large $\beta_2 \sim 10.5$, the internal configurations of the isotopic chain $^{112-122}\text{Ba}$ are of the form of two separated (identical) nuclei which are connected by a neck like configuration. The neck configurations contain simply the hydrogen isotopes $^2,3\text{H}$ or ^4He nucleus. As already noted in the Introduction, the existence of ^{12}C cluster inside the Ba nuclei has been of interest both from experimental and theoretical points of views. The important point is that ^{12}C cluster is formed inside the Ba nuclei, and are not from the neck region where $^2,3\text{H}$ or ^4He nuclei are shown to exist. In other words, ^{12}C constitutes the cluster structure of Ba nuclei.

IV. SUMMARY AND CONCLUSIONS

Concluding, we have calculated the gross nuclear properties and the nucleon density distributions for the isotopic chain $^{112-122}\text{Ba}$ using the deformed relativistic mean field (RMF) formalism with NL3 parameter set. The gross properties, like the binding energy, deformation parameter β_2 and the charge radius r_c , show qualitative similarity between the experimental and RMF calculated values. Analysing the nuclear density distributions, we get the internal or sub-structure of clusters in Ba isotopes which we find to consist mostly of $^{12,13}\text{C}$ and

several other clusters like ^1H , ^6Li and ^8Be . Some heavier clusters of Na, Cl, Mg, Ar and Ca are also obtained. With the increase of deformation ($\beta_2 \sim 10$ or 11), the Ba nucleus breaks (fissions) in to two symmetrical fragments, releasing from the neck region some clusters of hydrogen isotopes $^2,3\text{H}$ or ^4He . This is an interesting result of the RMF(NL3) technique for nuclear structure physics.

Clustering is also important for the decay of excited compound nuclei formed in nuclear reactions, where nuclei in the neck region could have correspondance with the measured fusion-evaporation residues consisting of light particles with $Z \leq 2$. We know from the Introduction above that todate the decay of $^{116,118,122}\text{Ba}^*$ compound nuclei in to intermediate

mass fragments (IMFs), and symmetric and near-symmetric fission fragments are measured [11, 12, 13, 14, 16], but the fusion-evaporation cross-sections are not yet measured.

V. ACKNOWLEDGMENTS

This work is supported in part by Council of Scientific & Industrial Research (No.03(1060)06/EMR-II), as well as the Department of Science and Technology, Govt. of India, project No. SR/S2/HEP-16/2005.

-
- [1] R. K. Gupta, S. Singh, R. K. Puri, and W. Scheid, Phys. Rev. C **47**, 561 (1993).
- [2] S. Kumar and R. K. Gupta, Phys. Rev. C **49**, 1922 (1994).
- [3] S. Kumar, D. Bir, and R. K. Gupta, Phys. Rev. C **51**, 1762 (1995).
- [4] S. Kumar, J. S. Batra, and R. K. Gupta, J. Phys. G: Nucl. Part. Phys. **22**, 215 (1996).
- [5] R. K. Gupta, *Proceedings of the 5th International Conference n Nuclear Reaction Mechanisms*, 1988, Varenna, Italy, edited by E. Gadioli (Ricerca Scientifica Educazione Permanente, Italy), p. 416.
- [6] S. S. Malik and R. K. Gupta, Phys.Rev. C **39**, 1992 (1989).
- [7] D. N. Peonaru, D. Schnabel, W. Greiner, D. Mazilu, and R. Gherghescu, At. Data. Nucl. Data. Table **48**, 231 (1991).
- [8] D. N. Peonaru, W. Greiner, and E. Hourani, Phys. Rev. C **51**, 594 (1995).
- [9] Yu. Ts. Oganessian, Yu. A. Lazarev, V. L. Mikheev, Yu. A. Muzychka, I. V. Shirokovsky, S. P. Tretyakova, and V.K. Utyonkov, Z. Phys. A **349**, 341 (1994).
- [10] A. Guglielmetti, B. Blank, R. Bonetti, Z. James, H. Keller, R. Kirchner, O. Klepper, A. Piechaczek, A. Plochocki, G. Poli, P. B. Price, E. Roeckl, K. Schmidt, J. Szerypo, and A. J. Westphal, Nucl. Phys. A **583**, 867 (1995).
- [11] J. Gomez del Campo, J. L. Charvet, A. D'Onofrio, R. L. Auble, J. R. Beene, M. L. Halbert, and H. J. Kim, Phys. Rev. Lett. **61**, 290 (1988).
- [12] J. Gomez del Campo, R. L. Auble, J. R. Beene, M. L. Halbert, H. J. Kim, A. D'Onofrio, and J. L. Charvet, Phys. Rev. C **43**, 2689 (1991).
- [13] J. Gomez del Campo, C. Baktash, H.-Q. Jin, D. Rudolph, A. D'Onofrio, F. Terrasi, G. de Angelis, M. De Poli, C. Fahlander, A. Gadea, D. R. Napoli, Q. Pan, P. Spolaore, L. De Acuna, D. Bazzacco, S. Lunardi, P.Pavan, C. Rossi-Alvarez, A. Buscemi, R. Zanon, A. De Rosa, L. Campajola, M. La Commara, G. Inglima, V. Roca, M. Romano, M. Sandoli, M. Romoli, A. Ordine, and D. Pierroutsakou, Phys. Rev. C **57**, R457 (1998).
- [14] M. La Commara, J. Gomez del Campo, A. D'Onofrio, A. Gadea, M. Glogowski, P. Jarillo-Herrero, N. Belcari, R. Borcea, G. de Angelis, C. Fahlander, M. Gorska, H. Grawe, M. Hellström, R. Kirchner, M. Rejmund, V. Roca, E. Roeckl, M. Romano, K. Rykaczewski, K. Schmidt, and F. Terrasi, Nucl. Phys. A **669**, 43 (2000).
- [15] R. K. Gupta, M. Balasubramian, R. Kumar, D. Singh, S. K. Arun, and W. Greiner, J. Phys. G: Nucl. Part. Phys. **32**, 345 (2006).
- [16] E. Bonnet, J. P. Wieleczko, J. Gomez del Campo, M. La Commara, S. Barlini, C. Beck, B. Borderie, R. Bougault, A. Chbihi, R. Dayras, G. De Angelis, J. D. Frankland, A. Galindo-Uribarri, T. Glodariou, V. Kravchuk, Ph. Lantesse, J. Moisan, N. Le Neindre, B. Martin, L. Nalpas, A. D. Onofrio, M. Parlog, D. Pierroutsakou, F. Rejmund, M. F. Rivet, M. Romoli, E. Rosato, R. Roy, D. Shapira, G. Spadaccini, B. Tamain, and M. Vigilante, Proc. State of the Art in Nuclear Cluster Physics (SOTANCP2008), Strasbourg (France), May 13-16, 2008, and Int. J. Mod. Phys. E **17**, 2359 (2008); J. P. Wieleczko, Private communication to one of us (RKG).
- [17] R. Kumar and R. K. Gupta, Phys. Rev. C **79**, 034602 (2009).
- [18] P. Arumugam, B. K. Sharma, S. K. Patra, and R. K. Gupta, Phys. Rev. C **71**, 064308 (2005).
- [19] R. K. Gupta, S. K. Patra, P. D. Stevenson, C. Beck, and W. Greiner, J. Phys. G: Nucl. Part. Phys. **35**, 075106 (2008).
- [20] S. K. Patra, R. K. Gupta, B. K. Sharma, P. D. Stevenson, and W. Greiner, J. Phys. G: Nucl. Part. Phys. **34**, 2073 (2007).
- [21] B. K. Sharma, P. Arumugam, S. K. Patra, P. D. Stevenson, R. K. Gupta, and W. Greiner, J. Phys. G: Nucl. Part. Phys. **32**, L1 (2006).
- [22] R. K. Gupta, S. K. Patra, P. D. Stevenson, and W. Greiner, Int. J. Mod. Phys. E **16**, 1721 (2007).
- [23] B. D. Serot and J.D. Walecka, Adv. Nucl. Phys. **16**, 1 (1986).
- [24] Y. K. Gambhir, P. Ring, and A. Thimet, Ann. Phys. (N.Y.) **198**, 132 (1990).
- [25] G. A. Lalazissis, J. König, and P. Ring, Phys. Rev. C **55**, 540 (1997).
- [26] S. K. Patra, F. H. Bhat, R. N. Panda, P. Arumugam, and R. K. Gupta, Phys. Rev. C **79**, 044303 (2009).
- [27] H. Flocard, P. Quentin, and D. Vautherin, Phys. Lett. **B46**, 304 (1973).
- [28] W. Koepf and P. Ring, Phys. Lett. **B212**, 397 (1988).
- [29] J. Fink, V. Blum, P.-G. Reinhard, J.A. Maruhn, and W. Greiner, Phys. Lett. **B218**, 277 (1989).
- [30] D. Hirata, H. Toki, I. Tanihata, and P. Ring, Phys. Lett. **B314**, 168 (1993).
- [31] G. Audi, A. W. Wapstra, and C. Thibault, Nucl. Phys. A **729**, 337 (2003).
- [32] B. Mohammed-Azizi and D. E. Medjadi, J. Phys. G: Nucl. Part. Phys. **35**, 035101 (2008).
- [33] P. Möller, J. R. Nix, W. D. Myers and W. J. Swiatecki, At. Data Nucl. Data Tables **59**, 185 (1995).
- [34] S. Goriely, F. Tondeur and J. M. Pearson, At. Data Nucl. Data Tables **77**, 311 (2001).